Full paper

A scalable, low-cost and robust photo-thermal fabric with tunable and programmable 2D/3D structures towards environmentally adaptable liquid/solid-medium water extraction

Peng Xiao[a,b], Jincui Gu[a,b], Chang Zhang[a], Feng Ni[a,b], Yun Liang[a,b], Jiang He[a,b], Lei Zhang[a,b,c], Jianyong Ouyang[c,*], Shiao-Wei Kuo[d], Tao Chen[a,b,**]

[a] Key Laboratory of Marine Materials and Related Technologies, Zhejiang Key Laboratory of Marine Materials and Protective Technologies, Ningbo Institute of Material Technology and Engineering, Chinese Academy of Sciences, Zhongguan West Road 1219, 315201, Ningbo, China
[b] University of Chinese Academy of Science, Beijing, 100049, China
[c] Department of Materials Science and Engineering, National University of Singapore, Singapore
[d] Department of Material and Optoelectronic Science, National Sun Yat-Sen University, 804, Kaohsiung, Taiwan

ARTICLE INFO

ABSTRACT

As a renewable and sustainable resource, solar energy exploited to conduct interfacial water evaporation has attracted considerable attention. However, conventional photo-thermal materials mainly focus on the issues of energy efficiency and multifunctionality, the lack of scalable, low-cost, flexible and washable features severely restrict the application from labs to industrialization. Significantly, owing to the low utilization of the spatial volume of the conventional two-dimensional (2D) evaporators, the development of editable and controllable 3D structures toward improved energy efficiency is highly desirable. Inspired by the traditional sewing clothes, herein, a functional photo-thermal fabrics with excellent scalable, washable and inexpensive features is designed to realize tunable and programmable 2D/3D structures, which enable the favorable in-plane and out-of-plane water extraction from liquid/solid medium. Since the polypyrrole (PPy) has favorable photo-thermal, stable features and strong interactions with the fibrous cotton, an *in situ* tunable oxypolymerization strategy was employed to construct PPy modified cotton fabric. The facile and robust approach enables the formation of a large-area PPy-modified cotton (PMC), which could function as a 2D generator for well-controlled in-plane water evaporation. Furthermore, the excellent sewable and editable features of the fabrics allow the programmable integration of these functional PMC building blocks into 3D system towards high-efficient out-of-plane solar vaporization. Specifically, the 3D design can adapt the photo-thermal fabrics to diverse environments with efficient purified water collection even from sand matrix.

1. Introduction

Water shortage that is regarded as a challenging global problem has aroused tremendous considerations [1]. To alleviate the water scarcity, extensive technologies are implemented to realize sewage purification and/or seawater desalination [2–7]. Among them, solar energy is expected to be a promising candidate owing to its sustainable and renewable features [8–10]. Significantly, superior to the traditional bulk solar distillation system, [11–13] solar driven interfacial evaporation has blossomed during the past few years, which enables highly efficient solar-to-thermal conversion [14–25]. Although considerable advances

are significantly achieved, challenges remain in achieving simple fabrication protocols, low-cost, favorable mechanical flexibility and washability [26,27]. More importantly, the conventional two-dimensional (2D) in-plane evaporation system with low space utilization severely restricts the solar-to-thermal conversion efficiency.

Based on the existing problem of energy efficiency, several recent researches were devoted to make their efforts in enhancing the light absorbance and/or improve the effective area of light absorption by transforming 2D films to three-dimensional (3D) networks [24,28–33]. Jiang et al. [34] prepared auricle-inspired 3D structure to prominently enhance the solar absorbance for effective water evaporation. Qu et al.

---

[35] constructed vertically aligned graphene pillar arrays through a high precision laser to increase the effective evaporation areas for achieving desirable solar steam generation. Notably, 3D structure is deemed to be a powerful and effective way to enhance the utilization of spatial volume in a confined system. However, the current 3D prototypes are still restricted to complicated fabrication process, limited sizes, undesirable mechanical strength and washability, *etc.* [36–38] Besides, it is challenging to realize editable and adjustable 3D structure in an updatable and correctable way. Considering that the flexible cotton fabric can be readily chemically modified, physically tailored, folded and sewn to a variety of desired 2D or 3D shapes, it is considered to be a preferred alternative to function as the editable and adaptable component element.

In nature, similar to the evaporation system, a transpiration behaviour of plants can start from the roots, subsequently the stems and finally to the leaves. Typically, the reversible switch behaviour between regeneration and withering of leaves can adapt themselves to diverse environmental conditions for sustainable survival [39]. Specifically, the natural materials based devices have the advantage of biodegradable, eco-friendly and commercially available properties, which have been widely adopted in various fields [40,41]. Actually, the specific functions and hierarchical structures of natural plants can inspire us to design some interesting and significant biomimetic materials and devices for efficient water purification [42–48]. Herein, a functional photo-thermal fabric with programmable 2D and 3D structure is designed to realize a controllable in-plane/out-of-plane solar steam generation in a scalable, cost-effective and programmable way. The achieved fabric represents favorable mechanically stable, washable and sewable features, which can be effectively sewn into desirable 3D configuration with highly transformable property. In our system, a large-area PPy modified cotton (PMC) fabric was readily achieved via controllable oxypolymerization strategy. The as-prepared PMC with desirable washability and mechanical strength demonstrates tunable 2D water evaporation rate through adjusting the relative content of PPy on cotton. Moreover, these 2D PMC could also function as the building blocks to construct hierarchical 3D structures. By adopting the conventional sewing technique, a cotton thread was employed to alternatively sew these functional PMC building blocks with pure cotton fabric to construct a programmable 3D system. Owing to the strong wicking effect of the cotton fabrics, water molecules from the bulk water can transport smoothly to the photo-thermal PMC surface for admirable solar vaporization. Furthermore, in practical applications, the functional PMC can realize a controllable transformation between 2D and 3D structure to adapt itself to variable environments. More interestingly, based on the specific structure of the 3D PMC, it can even extract seawater or other undrinkable water from the solid matrix for effective water evaporation, demonstrating significant potentials in some extreme conditions [17].

2. Results and discussions

The 2D photo-thermal PMC with tunable microstructures can also function as active building blocks and be tailored and sewn into editable 3D geometries to adapt to diverse environmental conditions. Compared with the planar 2D structure, the cone-like 3D structure is considered to effectively increase the light absorption due to the multiple light reflection. Note that the single cone-like structure can also elevate the utilization of spatial volume, resulting in higher improvement of effective surface area than that of the 2D one under the same projected area. It is noted that the resulted evaporation rate is calculated through dividing by the projected area for a normalized value. As a result, the 3D structure can exhibit higher water evaporation rate than that of the 2D one (Fig. S1) [34]. As a proof of concept, the 2D PMC with multiple hydrogen bond interactions between PPy and cotton fabric was folded/sewn to cone-shaped building blocks and subsequently integrated with cotton into a 3D structure (Fig. 1a). To form a

close-knit connection between 2D PMC and cotton fabric, a hydrophilic cotton thread was introduced to sew them together. Furthermore, a hierarchical framework that was defined as 3D PMC was fabricated by alternatively sewing PMC building blocks in the vertical direction. As displayed in Fig. 1b, the 3D PMC was composed of three parts, including cotton roots for water pumping, cotton stem for water transportation and cone-shaped PMC for light absorbance. Note that the plant-inspired 3D PMC can prominently improve the utilization of spatial volume. In addition, the hierarchical structure with reduced contacted area with water can effectively decrease the thermal conduction to the bulk water.

For the scalable production of 2D PMC, an oxypolymerization strategy was deployed in our system. The as-prepared PMC represented excellent mechanical strength and could be knotted into specific shapes with remarkable solar-to-thermal conversion under natural sunlight irradiation (Fig. 1c-d and Fig. S2). After an alternative sewing process, the PMC was combined with pure cotton fabric to form a bilayer structure (Fig. 1e and Fig. S3) [21]. To mimic the branched structures of plants for extensive light absorption, a hierarchical 3D architecture was designed by alternatively arranging these PMC building blocks into cotton-based stem (Fig. 1f). As expected, when the cotton-based stem was partially embedded into the water, the 3D PMC demonstrated a prominent temperature gradient under 1 sun illumination in the infrared images of Fig. 1g and Fig. S4. It is noted that the favorable solar-to-thermal effect derives from the efficient decoration of the PPy onto the surface of the cotton fabric, which could be clearly observed from the SEM images in Fig. 1h–j. The cross-sectional image further evidenced the successful modification of the functional polymer layers (Fig. 1k and Fig. S5).

The concrete PPy decoration procedures were schematically illustrated in Fig. 2a, in which a pure cotton fabric was firstly immersed into ferric solution ($FeCl_3/H_2O$) for the formation of coordination interaction, followed by a drying process under mild condition (Fig. S6). The ferric-modified cotton was then dipped in pyrrole solution for a series of reaction time [49]. Ultimately, the resulted PMC experienced a rigorous rinsing procedure to remove any dissociative Fe^{3+} or Fe^{2+}. Contributed to the accessible fabrication strategy, a large-area PMC can be successfully achieved and be further tailored into specific geometries with a scissor (Fig. 2b and c). Moreover, the endurance of PMC to the environment was also investigated in Fig. 2d and e. It was found that the resulted PMC can endure a series of treatments including rigorous soaking, ultrasonication and even severe washing in laundry detergent without any breakage. In addition, the chemical component of the PMC was further measured using ATR-FTIR spectrum. As displayed in Fig. 2f, compared with original cotton and ferric modified one, the existence of characteristic peak at $1542\,cm^{-1}$ strongly evidenced the successful modification of PPy on cotton surface. More importantly, the acquired PMC exhibited excellent mechanical strength, which was much stronger than some materials such as alumina foil, graphene aerogel, filtered membranes, *etc.* Despite the slightly weaker strength than that of original cotton, the tensile strength of PMC can still reach up to 44 MPa and maintain high stability even after extreme washing (Fig. 2g and Fig. S7) [50]. The high mechanical strength of PMC ensures the subsequent rigorous cutting, sewing and even washing procedures. In addition, the facile strategy allows the realization of low-cost functional fabric, which is approximately estimated. The fabricated photo-thermal fabric is expected to have a material cost of 2.75 $/m², which is competitive with the reported cost [51].

To optimize the photo-thermal performance of the PMC, a series of PMC samples with diverse oxypolymerization time were carefully studied. As displayed in Fig. 2h and Fig. S8, with the increase of reaction time ranging from 0.5 h to 24 h, the surface morphology of the cotton fabrics became much rougher than that of the original one, indicating that increasing PPy was formed on the cotton surface. In addition, thermal gravimetric analysis (TGA) measurement was conducted to further quantitatively investigate the amount of PPy on cotton surface.
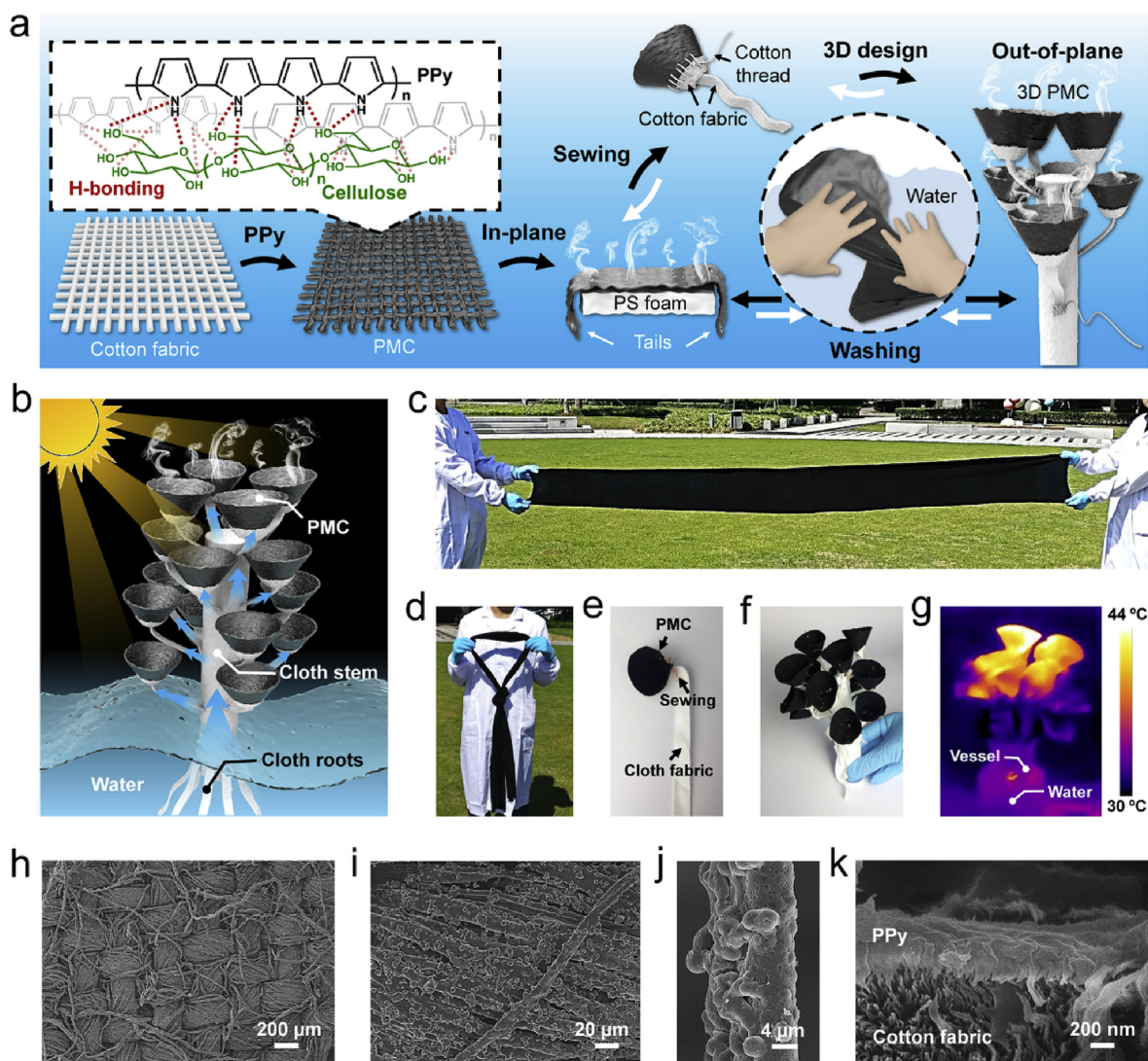
Fig. 1. a) Schematic illustration of functionalized cotton fabric as 2D/3D solar steam generators with favorable washable property. b) Schematic of the bio-inspired 3D hierarchical architectures for solar vaporization. c) Photo of large-scale PMC hybrid fabricated via an oxidation polymerization. d) The as-prepared PMC demonstrates good strength and flexibility, which can be knotted to specific shape. e) Through a sewing procedure, the pure cotton and PMC were incorporated together. f) A well-designed 3D architecture was exquisitely designed using cotton thread. g) Infrared image of the 3D architecture with roots immersed in the water under 1 sun. h-j) SEM images of the PMC surface. k) Cross-section image of the PMC, presenting apparent PPy layer on the cotton surface.

As displayed in Fig. S9, compared with the original cotton (Fig. S9a), the weight losses of PMC samples represent a gradual decrease tendency due to the increase of PPy reaction time (Fig. S9b). Specifically, it could be observed that the amount of PPy on cotton surface demonstrated an extremely slow increase after 6 h, which was also evidenced by the SEM images. This phenomenon may derive from the gradual decrease of the pyrrole monomers in the reaction solution. However, it can be found that the pores inside the cotton were inclined to decrease with the increase of PPy content, which may block the pathway of water transportation. Actually, light absorbance and water transportation pathway are both important factors that prominently affect the performance of water evaporation. As a result, it is important to balance the aforementioned factors.

Since the light absorbance is considered to be one of the crucial factors, the optical properties were explored using the ultraviolet–vis (UV–vis) near infrared (NIR) spectrum. As shown in Fig. 3a, compared with the high reflection of original cotton fabric, the resulted PMC demonstrated extremely low reflection in all spectral ranges. Especially, with the increase of reaction time, the reflectance value of the PMC decreased sharply and tended to be 1.68% and 3.1%, respectively, in

the visible and infrared (IR) regions. Furthermore, the extremely low reflectance and transmittance of the PMC ensure high light absorbance, resulting in a broadband absorption capability of over 98.3% of visible, and 96.3% of infrared solar irradiation (Fig. 3b). Besides, after decoration with PPy, the PMC with certain reaction time still maintained excellent capability of water absorption, allowing water transportation along the vertical direction of the PMC in several seconds (Fig. 3c). When irradiated under 1 sun, in comparison to the bulk water with almost constant temperature, it can exhibit a rapid temperature increase (Fig. 3d). Fig. 3e shows that the temperature of PMC can rise from 33 °C to 46.3 °C within 7 min. In contrast, the temperature of the bulk water increases slowly from 31.5 °C to 34.6 °C, indicating a lower solar-to-thermal conversion. Additionally, the temperature distribution in the vertical direction was also inspected under 1 sun (Fig. 3f). Fig. 3g demonstrates that temperature functions as a negative correlation with depth, in which the surface of PMC can rise up to 48.3 °C. The result indicates that the temperature is almost confined to the air-water interface without remarkable thermal diffusion to the water phase. Furthermore, the attainable temperature of PMC with different reaction time was measured in Fig. 3h, which represented a gradual temperature
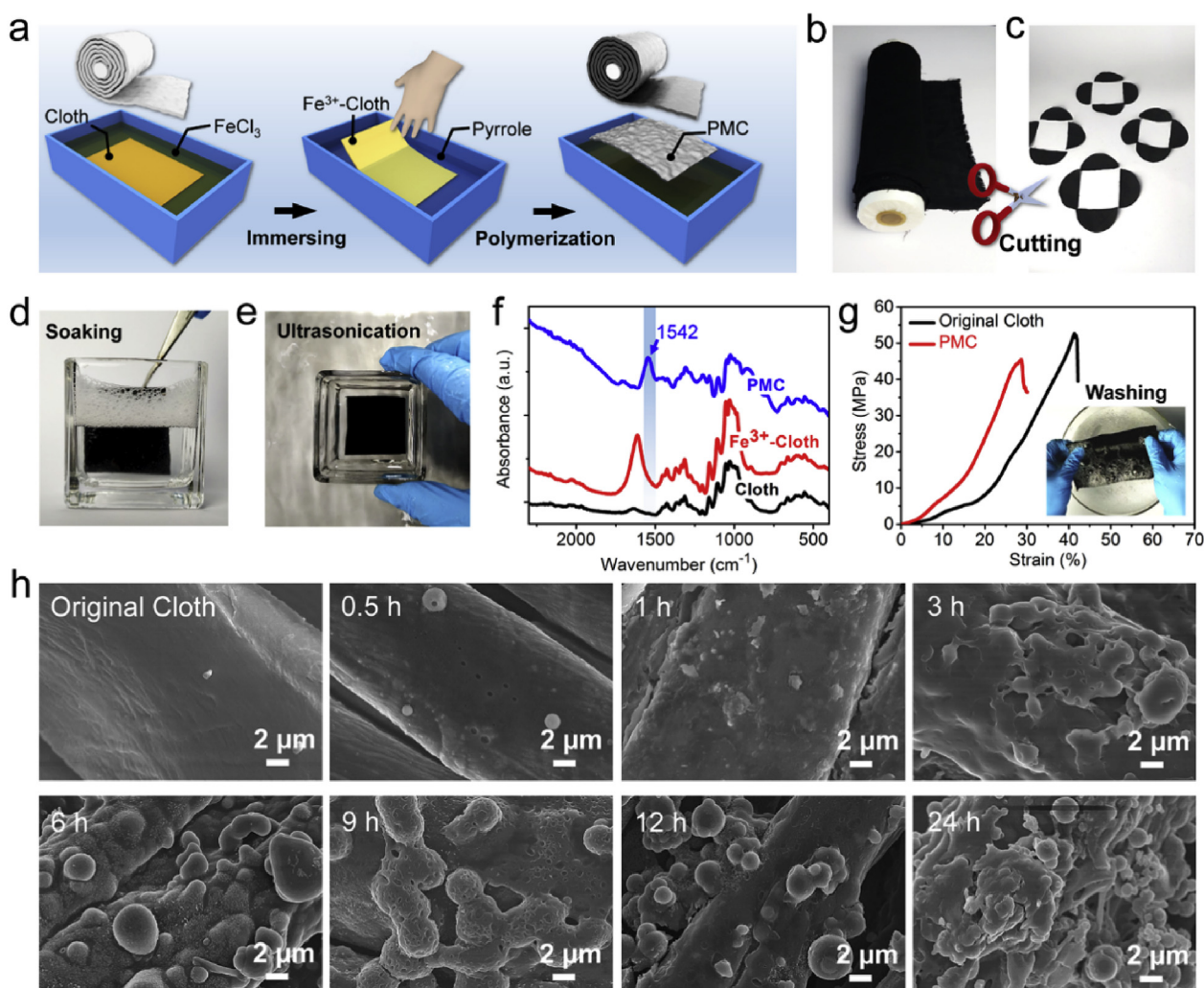
Fig. 2. a) Scheme of the fabrication of PMC by a ferric ion absorption and pyrrole-based oxypolymerization process. b) Scalable production of PMC after washing and drying procedures. c) It could be further cut into desired shapes. The PMC maintained a stable state without any breakage after d) Soaking and e) Ultrasonication. f) ATR-FTIR spectra of the original cloth, ferric treated cotton and PMC. g) Strain-stress curves before and after PPy modification. Inset: the PMC can even experience a rigorous washing procedure with excellent stability. h) SEM images of PMC with different reaction time.

increase and finally tended to be a stable value.

To further explore the performance of solar vaporization, 2D PMC samples with a series of reaction time were conducted in our experiments. Fig. 4a showed that 2D PMC was equipped with two tails for water pumping, which was attached onto the surface of a floating polystyrene foam. It can be clearly observed that a column of steam came out from the PMC surface under 5 sun illumination, indicating continuous and stable capability of water evaporation. As displayed in Fig. 4b and c, the performance of PMC samples with adjustable reaction time exhibited a parabolic trend, in which the evaporation rate of PMC in 9 h can reach up to $1.54 \, kg/m^2/h$. Note that when continued to increase the reaction time more than 9 h, the evaporation rate experienced an inevitable decrease, resulting from more PPy content severely blocking the water channels. As a result, PMC with 9 h was preferably selected in further experiments. To simulate different weather conditions such as cloudy and sunny days with different intensity, a variety of solar illumination ranging from 0.5 to $2.5 \, kW/m^2$ was conducted in Fig. 4d. The result indicates that a sustainable water supply can be readily achieved, exhibiting an excellent environment adaptability (Fig. 4e).

Moreover, the corresponding solar vaporization efficiency η with diverse illumination of the PMC was calculated using the following equation that defined as $\eta = mh/I_{sun}$, in which m denotes the mass flux,

h is the total enthalpy of the liquid-liquid sensible heat and liquid–vapour latent heat and I_{sun} is the total power of solar illumination. The calculated solar thermal efficiency in Fig. 4f demonstrates a gradual increase trend ranging from 61.2% in 0.5 sun to 96% in 2.5 sun. Notably, the desalination performance was also evaluated by using simulated seawater in our system. Specifically, after distillation, the concentration of ions including the Na^+, Mg^{2+}, Ca^{2+}, K^+, B^{3+} and Sr^{2+} was significantly reduced to 0.51, 0.131, 0.052, 0.537, 0.305 and 0.006 mg/L with an average rejection rate of 98.8% (Fig. 4g and h). The calculated value is substantially below the World Health Organization (WHO) standard, demonstrating a significant potential for purified water collection. Furthermore, the salt-rejecting performance was explored in our system, which was exposed to the solar with 1.5 sun for 8 h in a simulated seawater. As expected, there were some salt particles precipitated from the PMC surface. More importantly, due to the favorable water absorption capability of the PMC, when it was allowed to cool overnight, almost no salt was observed (Fig. 4i).

Since the 2D PMC represents favorable performance of in-plane water evaporation, these functional PMC building blocks can further expand themselves to 3D direction for harvesting more sunlight. It is noted that the 2D and 3D PMC can adapt to variable environments for desirable water evaporation. When the evaporation chambers are limited to the high cost and confined size, the efficient utilization of spatial
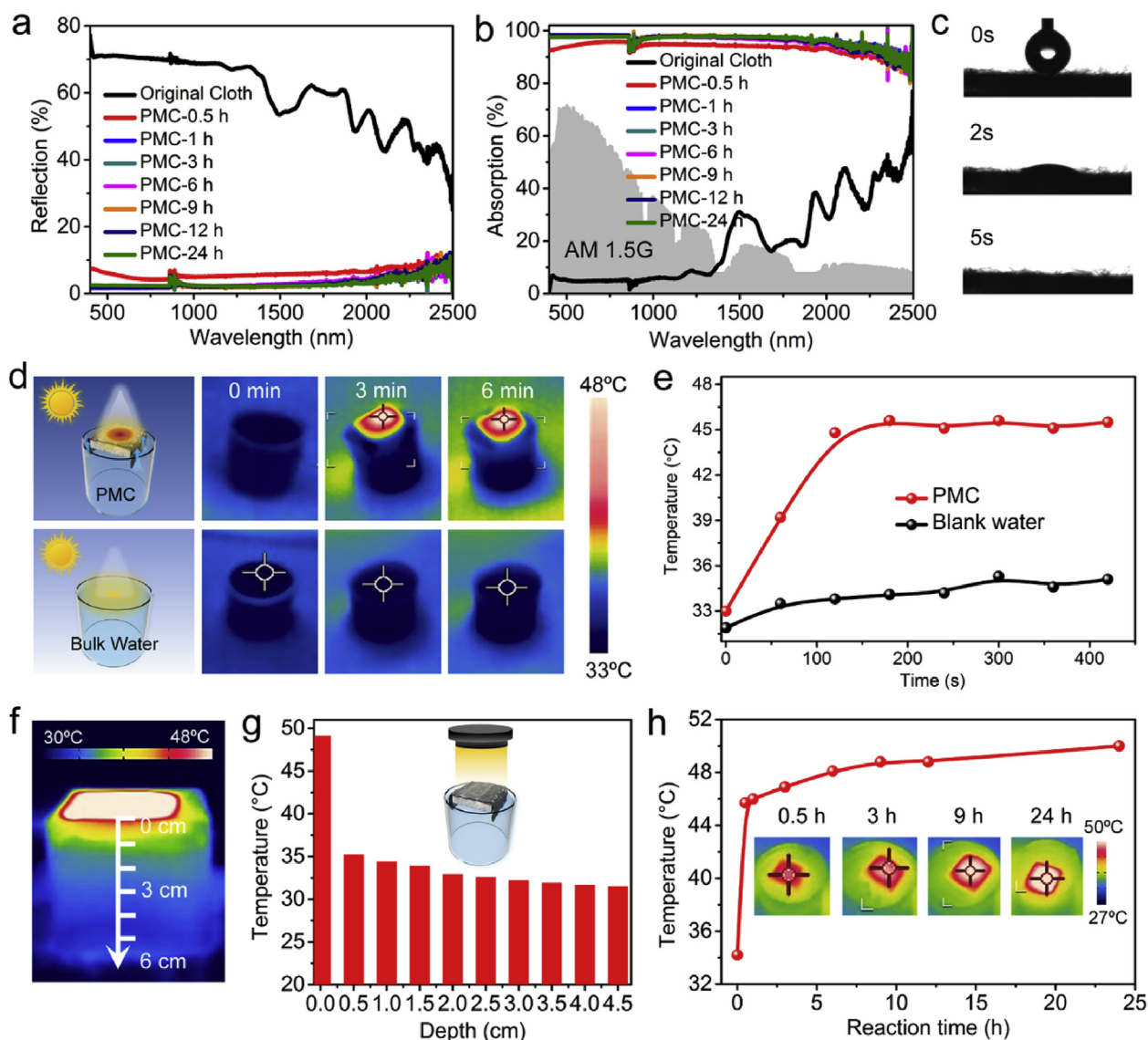
Fig. 3. a) Reflection versus wavelength curves of original cloth and PMC with different reaction time. b) Solar spectral irradiance (AM 1.5 G) and absorption curves of original cloth and PMC with different reaction time. c) Water contact angle (WCA) of the PMC, showing good capability of water absorption. d) IR images with and without PMC under 1 sun, showing a remarkable surface temperature difference. e) The corresponding temperature versus time curves. f) IR picture of PMC under 1 sun. g) The temperature versus depth column on the vertical direction. h) Temperature versus samples with different pyrrole reaction time curve.

volume is considered as an effective way. The rolls of 2D PMC fabric can be transported to certain place and assembled to the 3D structure for enhanced evaporation. However, when the roof height of low-cost chamber is too low to accommodate the 3D PMC, the 2D one is highly preferred, which represents more material utilization efficiency and simple assembly procedures than the 3D one (Fig. S10). As illustrated in Fig. 5a, 2D PMC (zone I) and cotton (zone II) performed as the light absorber and thermal isolation/water transportation, respectively, which could be employed as an isolated building block. To fabricate a hierarchical 3D PMC, PMC building blocks were integrated to the cotton-based stem surface to make the best of the confined space with the aid of cotton thread (Fig. 5b). When embedded into the water, the achieved 3D PMC with specific plant-like steam can drastically reduce the possible thermal conduction to the bulk water (Fig. 5c). With the increase of irradiation time under 1 sun, the 3D PMC system exhibited a prominent temperature increase, in which the temperature up to 43.5 °C was mostly limited to the PMC layers (Fig. 5d). Compared with the 2D PMC with plane structure, the 3D one demonstrated a relatively lower surface temperature due to non-vertical light incidence on the

cone-like structure (Figs. S11a and 11b). As a result, the corresponding thermal convection and radiation of 3D PMC to the environment are expected to be lower than that of the 2D one (Fig. S11c).

Furthermore, owing to the hierarchical structure, the cotton fabric based stem can effectively reduce the thermal loss to the bulk water. Note that there are four PMC building blocks in one layer. The performance of solar vaporization could be readily adjusted by changing the PMC layers. In our work, the projected area measured from the top view was employed to calculate the value of water evaporation (Fig. S12a). Since the simulated solar light intensity could have a drastic change along the vertical direction of the 3D PMC, the top layer of the 3D structure was defined as the base level to adjust the required solar intensity (Fig. S12b). Nevertheless, the other parts of the 3D PMC resulted in decreased light intensity. Based on this standard, water evaporation experiments of 3D PMC were conducted. As shown in Fig. 5e and f, the evaporation rate demonstrated an increasing trend ranging from 1.51 kg/m^2 for 1 layer to 3.37 kg/m^2 for 4 layers. Specifically, it is noted that the area used in the efficiency formula is the projected area of the 3D PMC, which is much smaller than the actual evaporation area
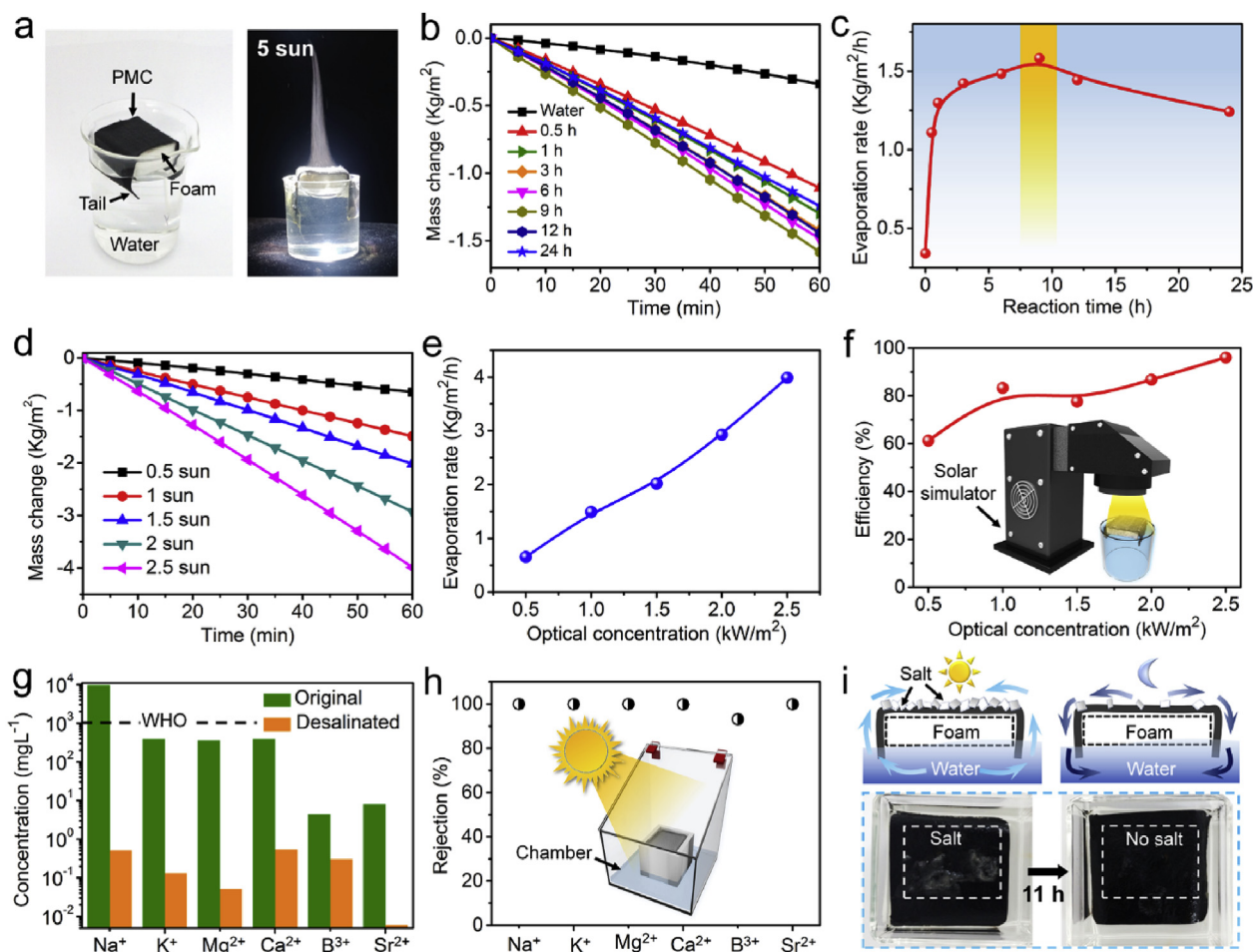
Fig. 4. a) Photographs of PMC on a floating foam with two tails for water pumping and water vapor can be clearly observed under 5 sun. b) Mass change versus time curves of blank water and PMC with different reaction time under 1 sun irradiation (1 kW/m²). f) Mass change versus reaction time curve, showing a maximum evaporation rate at 9 h. d) Mass change of sample with 9 h reaction versus optical concentration curves. e) The corresponding evaporation rate under different optical concentration. f) Solar steam efficiencies under different sun irradiation. g) The ion concentration of six simulated seawater samples before and after desalination. h) The ion rejection of seawater sample. i) Photos of sample with apparent salt aggregates after long time irradiation and the salts were extracted to the seawater after one night (about 11 h).

(Fig. S13). Given the specific structure of the plant-like 3D configuration, the circumcircle area of the projected area is acquired to further calculate the water evaporation rate of the 3D PMC. Actually, the projected area can also be regarded as the occupied area. For other 3D configurations, the projected area depends on the shape and size of the 3D models. The remarkable improvement of the water evaporation for the 3D PMC results from the enhanced light absorption and increased specific surface area. Under the same project, with the increase of layers, the effective surface area per unit area presents a gradual increase trend, resulting in accelerated water evaporation. Considered the limited evaporation chambers in practical application, the effective utilization of spatial volume can prominently increase the efficiency of purified water collection, which is superior to the 2D structure.

To further demonstrate the relationship between enhanced utilization of spatial volume of 3D PMC and accelerated water evaporation rate, the 3D PMC is simplified as a cylinder. Moreover, the volume of cylinder is divided into four parts, in which one layer takes up one quarter of the total volume. Enhancement factor (EF) that is denoted as the evaporation rate ratio of 3D PMC with different layers and 3D one with one layer is introduced to illustrate the correlation between accelerated evaporation rate and spatial volume. As displayed in Fig. S14, with the increase of utilization of spatial volume, EF represents a remarkable increase tendency. However, when further increased the layers of PMC, the effective light absorption areas may not present a

prominent increase due to the unexpected space barrier among these PMC. This phenomenon may derive from the saturated irradiation area, which cannot allow the light to penetrate into the underside of the PMC building blocks (Fig. S15). In addition, the evaporation experiments of 5 and 6 layers of 3D PMC were also conducted. As shown in Fig. S16, the calculated EF value demonstrates two step increase process, including a relatively quick increase for 3D PMC within 4 layers and a slow increase for 3D one with more than 4 layers. Attributed to the extremely low light absorption of the additional layers for 5 and 6 layers, the solar-driven water evaporation for the newly added layers is severely limited. However, the dark water evaporation rate for the additional layers is not significantly affected by the sunlight irradiation. To further evidence the light obstruction effect, the evaporation performance of PMC with different layers in dark condition is also investigated. As shown in Fig. S17, there is a linear correlation between dark evaporation rate and 3D PMC ranging from 1 to 6 layers. The result illustrates that the obstruction effect of the light severely limits the evaporation rate of 3D PMC with more than 4 layers. As a result, for 3D PMC with more layers may result in the prominently weakened increase of water evaporation rate. In addition, the effect of incident angles on the 3D PMC evaporation performance is also discussed. Compared with 2D structure with constant illumination area, the effective area of 3D one can experience a dynamic change process that depends on the changeable illumination angles. In this work, the cone-
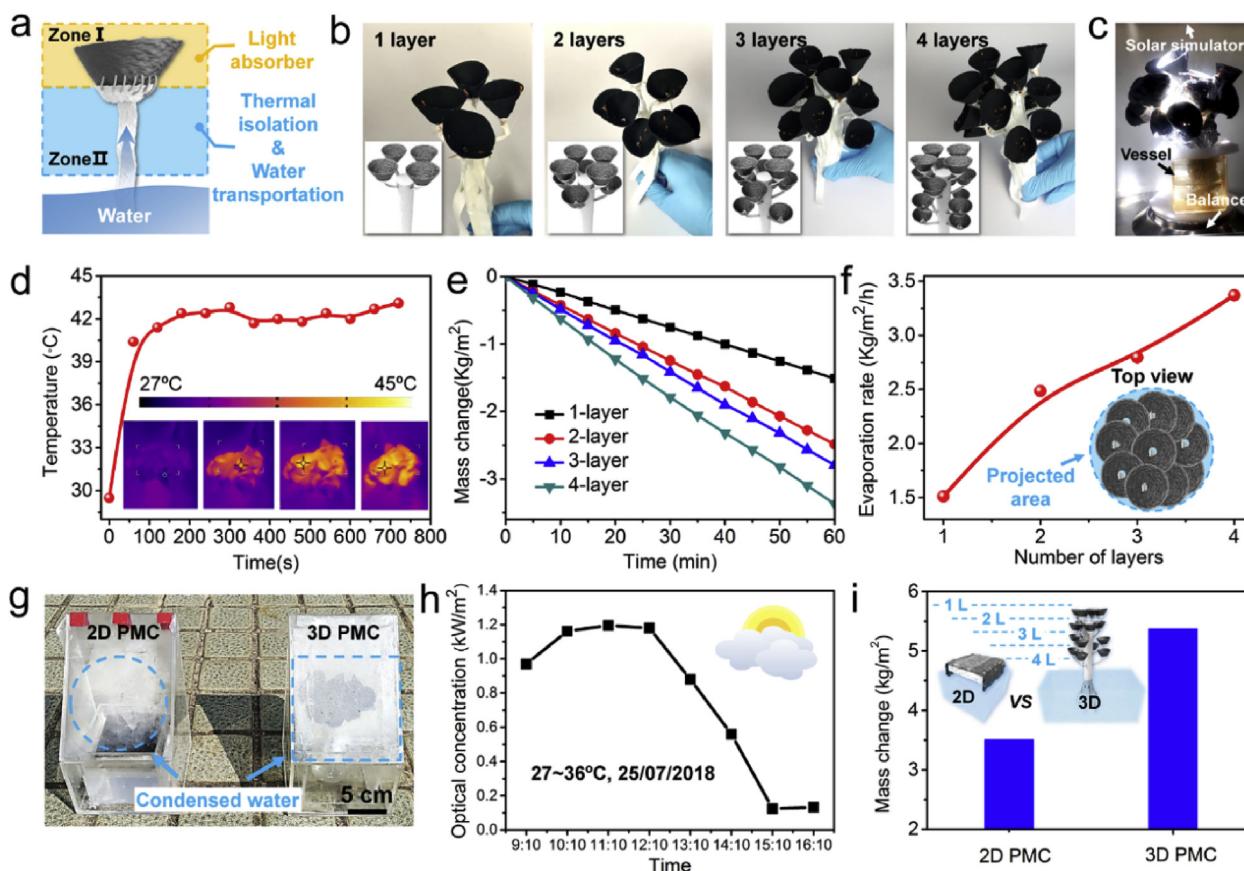
Fig. 5. a) Sketch of work mechanism of the 3D PMC with typical light absorber layer and water transportation layer. b) Pictures of 3D PMC sewed with different layers to realize well-controlled solar vaporization. c) 3D PMC with 4 layers under 1 sun illumination. d) Temperature versus time curve of 3D PMC with 4 layers under 1 sun. Inset: corresponding 2D IR images. e) Mass change versus time curves of 3D PMC with different layers. f) Evaporation rate curve of 3D PMC with different layers. g) Photo of the outdoor evaporation experiments with 2D and 3D PMC in sealed chambers. h) Solar illumination intensity versus time curve in a sunny day. i) Mass change of the acquired purified water by 2D and 3D PMC.

like units in the symmetric 3D PMC are provided with different orientations, which are considered to further decrease the negative effects from the light obstruction (Fig. S18). It is expected that rational design of 3D structure may efficiently reduce the negative effect of incident angles. Therefore, more refined structural design and geometric simulation for utmost utilization of spatial volume will be deeply studied in further work, which is not discussed in this work.

As a promising platform for efficient solar steam generation, 2D PMC and 3D PMC were both employed to conduct outdoor contrast experiments. From Fig. 5g it can be observed that compared with 2D PMC, the 3D one enabled more water to condense on the roof of the sealed chamber. The controlled experiment was carried out from 09:10 to 16:10 with an average solar heat flux of ~0.78 kW/m^2 in a cloudy day (Fig. 5h). As a result, the 3D PMC allowed an average water evaporation rate of ~0.77 kg/m^2/h, which is 1.54 times higher than that of 2D one with the value of ~0.50 kg/m^2/h. In practical applications, the 2D and 3D PMC are usually confined in a sealed chamber with considerable light reflection of the roof the chamber. More importantly, with the increase of the relative humidity in the chamber, the high humidity (usually approaching to 100%) can severely weaken the water evaporation. Compared with the value measured in the lab, both of the 3D and 2D structures demonstrated a weakened evaporation efficiency (Fig. 5i) [33]. Significantly, the achieved 3D PMC can also present a desirable wicking effect to reduce the potential salt aggregation. When enough NaCl crystals were added onto the surface of the PMC that partly immersed into the simulated seawater, the salt could completely sink into the bulk seawater overnight (Fig. S19). In addition, to explore the feasibility of this 3D concept, a large 3D configuration with the

diameter of ~15 cm was fabricated and further employed to conduct the outdoor evaporation experiment due to limit of solar simulator. As shown in Fig. S20, it was found that the well-established 3D tree-like structure was placed on a large-scale evaporation device, in which the evaporation rate with a value of ~1 kg/m^2/h could be achieved under the average light intensity of ~0.86 kW/m^2.

Natural plants can extract water from sand or soil matrix, which makes them adapt to the variable environments. This interesting phenomenon has aroused us to direct the 3D PMC from the bulk water to the sand matrix for proposed water collection. As illustrated in Fig. 6a, the 3D HPG was supported with stainless steel framework and implanted into the simulated sand environment. It is noted that the simulated sand/water mixture was prepared with the water content of about 23.7 wt%, in which no apparent flowing water was observed on the sand surface (Fig. S21). Attributed to the strong wicking effect of the cotton fabric-based roots and stems, the water inside the sand could be readily extracted to the PMC surface for effective solar-to-thermal conversion. In the controlled experiments, 2D PMC on polystyrene foam with two PMC tails was partially embedded into the sand for water pumping. To mimic the behavior of plants, the 3D PMC was rooted in the deep sand matrix, enabling the roots to extend deeply into sand for water absorption. For the comparative experiments, the tails of 2D PMC and the stem of 3D one were embedded into the same depth in the outdoor experiments (Fig. S22). The specific 3D structure ensures a continuous and effective water transportation from the sand substrate to the photo-thermal PMC layers (Fig. 6b). When sealed in the chamber prototype with the same projected area, it could be found that there were much larger water droplets condensed, converged and
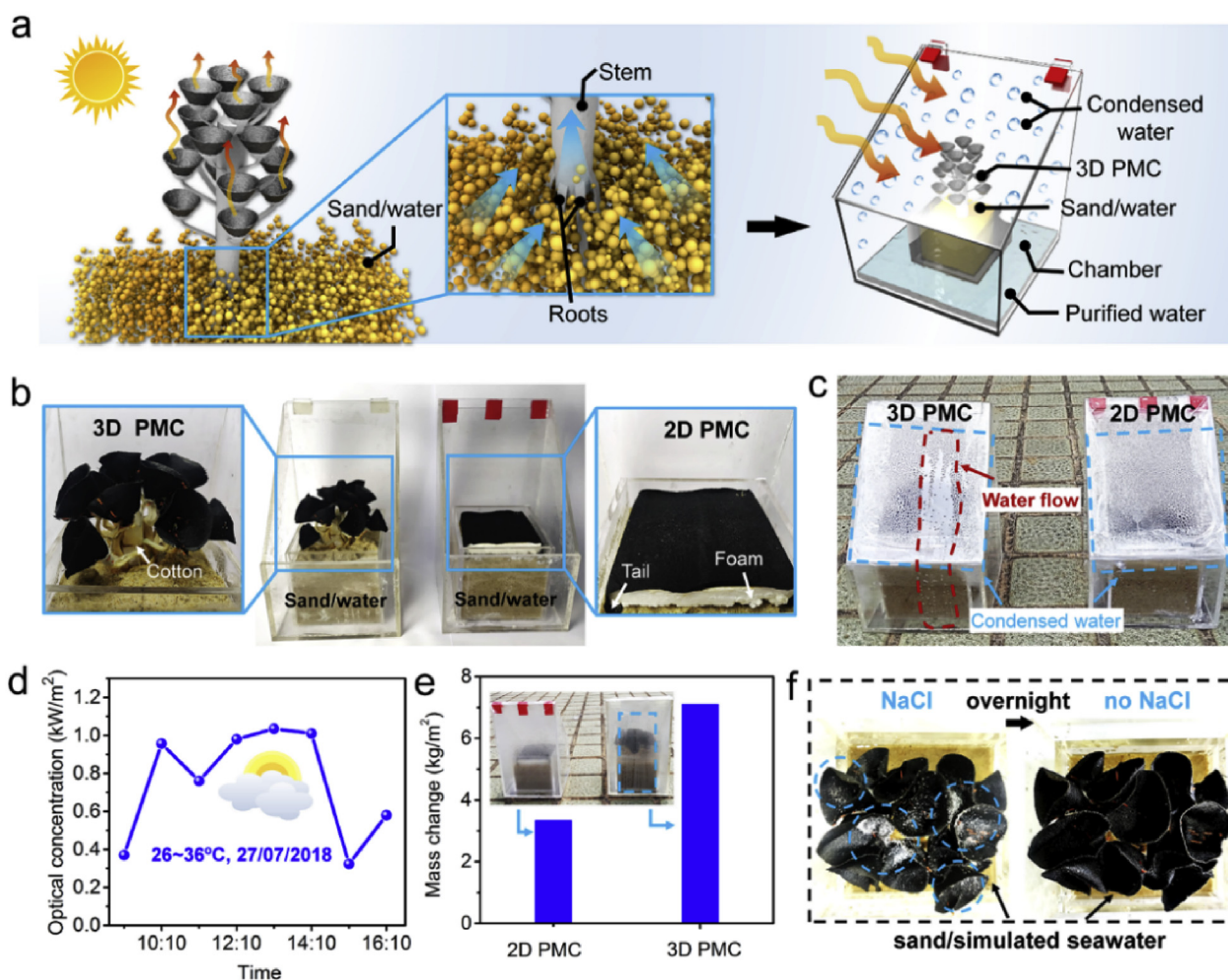
Fig. 6. a) Schematic illustration of the 3D PMC embedded into the sand/water matrix for extracting the water from the ground. b) Photos of contrast experiments of 2D and 3D PMC to extract purified water from the simulated sand environment. c) The outdoor solar vaporization experiments in sealed chambers under natural sunlight, exhibiting a prominent water flow from the chamber of 3D PMC. d) Solar intensity versus time curve in a cloudy day. e) Mass change of the purified water by 2D and 3D PMC from simulated sand. f) Pictures of the wicking effect of 3D PMC by putting enough solid NaCl to a saturated state on the cone-shaped PMC surface, in which the salt can fully sink into the sand overnight.

consequently flowed in the 3D PMC system, indicating a robust capability of high-efficient water collection (Fig. 6c). The outdoor experiment was conducted from 09:10 to 16:10 under natural sunlight with average solar heat flux of ~0.75 kW/m^2 in a cloudy day (Fig. 6d). The normalized collected water of 3D and 2D PMC was 7.11 and 3.35 kg/m^2, respectively (Fig. 6e). Specifically, an enhancement factor that was denoted as the evaporation rate ratio of 3D and 2D PMC was introduced to manifest the promotion efficiency, representing a prominent improvement of 2.12 under the same condition. Note that compared with the bulk water, the sand/water mixture can remarkably enhance the solar-to-thermal conversion (Fig. S23). The phenomenon derives from the efficient water isolation effect by sand particles, resulting in enhanced water evaporation rate of 3D PMC in sand matrix even under the similar solar intensity. Owing to the favorable wicking effect of the cotton fabrics, the salt from the simulated water is difficult to aggregate on the surface of the 3D PMC (Fig. S24). To further investigate the wicking of the 3D structure, sufficient NaCl crystals were sprinkled on the PMC surface until a saturated state was achieved. As displayed in Fig. 6f, white salt particles could be easily observed on the cone-shaped PMC surface. Due to the excellent capability of water absorption of the 3D PMC, the solid salts can be readily and fully dissolved into the simulated seawater in the sand matrix overnight.

Specifically, some potential problems including durability, recyclability and environmental protection of the achieved fabric should also be considered in the design of photo-thermal materials. Owing to the favorable stability of the PPy, it can function as the anticorrosion layer. In this work, it is observed that the PMC can still work effectively after 9 months (Fig. S25). However, the potential degradation is still inevitable in the long-term outdoor applications. It is expected that the subsequent multiple PPy modification can be an alternative method for cyclic utilization. Furthermore, for the problem of environment pollution, note that the PMC is composed of two environmentally non-toxic ingredients, including the biocompatible PPy and degradable cellulose. Given the broad applications of PPy, the PMC can be treated to be environmentally sound via the current mature techniques.

3. Conclusions

In conclusion, a functional photo-thermal fabric with tunable and programmable 2D/3D geometries was constructed through a scalable, low-cost and high-efficient way. The achieved 2D PMC demonstrated tunable in-plane water evaporation by adjusting the oxypolymerization time, in which the light absorption and water transportation are balanced to acquire an optimized 2D steam generator. Furthermore, the 2D PMC and original cotton fabric were alternatively sewn together to be specific building blocks, which were further edited to realize a 3D PMC. The well-designed 3D PMC demonstrates excellent mechanically flexible, washable and salt-rejecting properties, enabling a high-

efficient out of plane solar steam generation. Specifically, the PMC-based generators can realize a controllable transition from 2D to 3D structures to effectively adapt to diverse conditions, representing significant potentials in water distillation and/or sewage purification under some extreme conditions.

4. Experimental section

4.1. Fabrication of PPy modified cotton fabrics

A commercially available cotton fabrics was thoroughly rinsed with acetone and ethanol to remove any oily residues, followed by deionized water washing and drying procedures. The resulted cotton fabric was firstly immersed into the $FeCl_3 \cdot 6H_2O$ solution (1 mol/L) to absorb sufficient ferric for 1 h. Subsequently, the ferric-decorated cotton was further immersed into the pyrrole solution (0.2 mol/L) for a series of reaction time. Finally, for a certain oxypolymerization time, the polypyrrole modified cotton was rigorously washed with deionized water to remove any Fe^{3+}/Fe^{2+}, unstable polymer and dried in an oven for 2 h. To achieve a favorable capability of water absorption, the as-prepared samples were further treated with oxygen plasma for 100 s using a plasma cleaning equipment (TS-P120, Shenzhen Tonson High-tech) with an oxygen flow of 0.15 L/min.

4.2. Preparation of 3D PMC

Firstly, the achieved PMC was cut into semicircle and sewn into a cone-shaped 3D structure with apex angle of 56° (that is denoted as cone-shaped PMC) to substantially absorb the irradiated solar energy. Secondly, the resulted cone-shaped PMC was further combined with original cotton that acted as torus and branched stem) to form an isolated PMC building block. Finally, these PMC building blocks were orderly integrated into the cotton-based stem for the architecture 3D PMC.

4.3. Solar vaporization experiments

Square-shaped 2D PMC with two tails and 3D PMC were both employed to conduct the water evaporation experiments. The 2D and 3D PMC were floated on the water surface through a polystyrene foam. Especially, the 3D one was partially embedded into the foam, ensuring a good water transportation to the PMC surface. The resulted solar steam generators were further irradiated by a solar simulator (HM-Xe500W) equipped with the optical filter for AM 1.5G spectrum. The mass changes were measured by electronic balance with an accuracy of 0.0001 g at constant temperature and humidity. It is noted that the total enthalpy that is denoted as h includes sensible heat and latent heat. In our work, the sensible heat can be calculated using the specific heat of 4.2 J/g/K from initial temperature to the final temperature. The latent heat of water vaporization is 2.26 kJ/g. When calculated the evaporation efficiency, the average evaporation rate of pure water in the dark should be subtracted to acquire the actual water evaporation value of the as-prepared generators.

4.4. Characterization

Field Emission Scanning Electron Microscope (FE-SEM) images were obtained with a FE scanning electron microanalyzer (Hitachi-S4800, 4 kV). Attenuated total Reflectance Fourier transform infrared (ATR-FTIR) Spectroscopy (Cary 610, Agilent Technologies, Australia) was employed to characterize the structural information before and after PPy modification. Optical Transmittance of the films was probed using UV–vis–NIR spectra, which were obtained with a Lambda 950 spectrophotometer from PerkinElmer Instrument Co., Ltd. USA. Static water contact angles were measured at room temperature using the sessile drop method and image analysis of the drop profile by using the

instrument (OCA-20, Dataphysics) with a charge-coupled device camera and an image analysis processor. The universal testing machine (Instron 5567) was used to perform the tensile strength tests with a speed of 3 mm/s. An IR camera (FLIR E8) with a resolution of 320×240 pixels was employed to realize a real-time recording of the surface temperature and IR images of the PMC samples. Thermal Gravity Analysis (TGA) was carried out on a Pyris Diamond TG/DTA instrument from 30 to 1000 °C at a heating rate of 20 °C min^{-1}.

Appendix A. Supplementary data

Supplementary data to this article can be found online at https://doi.org/10.1016/j.nanoen.2019.104002.

References

[1] M.A. Shannon, P.W. Bohn, M. Elimelech, J.G. Georgiadis, B.J. Marinas, A.M. Mayes, Nature 452 (2008) 301–310.
[2] M. Elimelech, W.A. Phillip, Science 333 (2011) 712–717.
[3] J. Gu, P. Xiao, Y. Huang, J. Zhang, T. Chen, J. Mater. Chem. A 3 (2015) 4124–4128.
[4] J.C. Gu, P. Xiao, J. Chen, J.W. Zhang, Y.J. Huang, T. Chen, ACS Appl. Mat. Interfaces 6 (2014) 16204–16209.
[5] J. Gu, P. Xiao, J. Chen, F. Liu, Y. Huang, G. Li, J. Zhang, T. Chen, J. Mater. Chem. A 2 (2014) 15268–15272.
[6] L. Zhang, J.C. Gu, L.P. Song, L. Chen, Y.J. Huang, J.W. Zhang, T. Chen, J. Mater. Chem. A 4 (2016) 10810–10815.
[7] L. Zhang, X.H. Zha, G. Zhang, J.C. Gu, W. Zhang, Y.J. Huang, J.W. Zhang, T. Chen, J. Mater. Chem. A 6 (2018) 10217–10225.
[8] H.M. Qiblawey, F. Banat, Desalination 220 (2008) 633.
[9] C. Li, Y. Goswami, E. Stefanakos, Renew. Sust. Energ. Rev. 19 (2013) 136–163.
[10] N.S. Lewis, Science 315 (2007) 798.
[11] A.E. Kabeel, S.A. El-Agouz, Desalination 276 (2011) 1–12.
[12] O. Neumann, A.S. Urban, J. Day, S. Lal, P. Nordlander, N.J. Halas, ACS Nano 7 (2013) 42–49.
[13] N.J. Hogan, A.S. Urban, C. Ayala-Orozco, A. Pimpinelli, P. Nordlander, N.J. Halas, Nano Lett. 14 (2014) 4640–4645.
[14] J. Wang, Y.Y. Li, L. Deng, N.N. Wei, Y.K. Weng, S. Dong, D.P. Qi, J. Qiu, X.D. Chen, T. Wu, Adv. Mater. 29 (2017) 1603730.
[15] H. Ghasemi, G. Ni, A.M. Marconnet, J. Loomis, S. Yerci, N. Miljkovic, G. Chen, Nat. Commun. 5 (2014) 4449.
[16] K. Bae, G.M. Kang, S.K. Cho, W. Park, K. Kim, W.J. Padilla, Nat. Commun. 6 (2015) 10103.
[17] M.W. Zhu, Y.J. Li, G. Chen, F. Jiang, Z. Yang, X.G. Luo, Y.B. Wang, S.D. Lacey, J.Q. Dai, C.W. Wang, C. Jia, J.Y. Wan, Y.G. Yao, A. Gong, B. Yang, Z.F. Yu, S. Das, L.B. Hu, Adv. Mater. 29 (2017) 1704107.
[18] L. Zhang, B. Tang, J. Wu, R. Li, P. Wang, Adv. Mater. 27 (2015) 4889–4894.
[19] L. Zhou, Y. Tan, J. Wang, W. Xu, Y. Yuan, W. Cai, S. Zhu, J. Zhu, Nat. Photonics 10 (2016) 393–398.
[20] Y. Liu, S. Yu, R. Feng, A. Bernard, Y. Liu, Y. Zhang, H. Duan, W. Shang, P. Tao, C. Song, T. Deng, Adv. Mater. 27 (2015) 2768–2774.
[21] Q. Jiang, L. Tian, K.-K. Liu, S. Tadepalli, R. Raliya, P. Biswas, R.R. Naik, S. Singamaneni, Adv. Mater. 28 (2016) 9400–9407.
[22] G. Ni, Nat. Energy 1 (2016) 16126.
[23] P. Zhang, J. Li, L. Lv, Y. Zhao, L. Qu, ACS Nano 11 (2017) 5087–5093.
[24] X.Y. Zhou, F. Zhao, Y.H. Guo, Y. Zhang, G.H. Yu, Energy Environ. Sci. 11 (2018) 1985–1992.
[25] Y.B. Yang, X.D. Yang, L.N. Fu, M.C. Zou, A.Y. Cao, Y.P. Du, Q. Yuan, C.H. Yan, ACS Energ. Lett. 3 (2018) 1165–1171.
[26] M. Gao, L. Zhu, C.K. Peh, G.W. Ho, Energy Environ. Sci. 12 (2019) 841–864.
[27] Z.Y. Deng, J.H. Zhou, L. Miao, C.Y. Liu, Y. Peng, L.X. Sun, S. Tanemura, J. Mater. Chem. A 5 (2017) 7691–7709.
[28] X. Li, R. Lin, G. Ni, N. Xu, X. Hu, B. Zhu, G. Lv, J. Li, S. Zhu, J. Zhu, Nat. Sci. Rev. 5 (2018) 70–77.
[29] S. Hong, Y. Shi, R. Li, C. Zhang, Y. Jin, P. Wang, ACS Appl. Mat. Interfaces 10 (2018) 28517–28524.
[30] H.M. Song, Y.H. Liu, Z.J. Liu, M.H. Singer, C.Y. Li, A.R. Cheney, D.X. Ji, L. Zhou, N. Zhang, X. Zeng, Z.M. Bei, Z.F. Yu, S.H. Jiang, Q.Q. Gan, Adv. Sci. 5 (2018) 1800222.
[31] X. Li, J. Li, J. Lu, N. Xu, C. Chen, X. Min, B. Zhu, H. Li, L. Zhou, S. Zhu, T. Zhang,

J. Zhu, Joule 2 (2018) 1331–1338.

[32] Y.J. Li, T.T. Gao, Z. Yang, C.J. Chen, W. Luo, J.W. Song, E. Hitz, C. Jia, Y.B. Zhou, B.Y. Liu, B. Yang, L.B. Hu, Adv. Mater. 29 (2017) 1700981.

[33] F. Zhao, X. Zhou, Y. Shi, X. Qian, M. Alexander, X. Zhao, S. Mendez, R. Yang, L. Qu, G. Yu, Nat. Nanotechnol. 13 (2018) 489–495.

[34] Y. Wang, C. Wang, X. Song, M. Huang, S.K. Megarajan, S.F. Shaukat, H. Jiang, J. Mater. Chem. A 6 (2018) 9874–9881.

[35] P.P. Zhang, Q.H. Liao, H.Z. Yao, H.H. Cheng, Y.X. Huang, C. Yang, L. Jiang, L.T. Qu, J. Mater. Chem. A 6 (2018) 15303–15309.

[36] T. Li, H. Liu, X.P. Zhao, G. Chen, J.Q. Dai, G. Pastel, C. Jia, C.J. Chen, E. Hitz, D. Siddhartha, R.G. Yang, L.B. Hu, Adv. Funct. Mater. 28 (2018) 1707134.

[37] G.H. Liu, J.L. Xu, K.Y. Wang, Nano Energy 41 (2017) 269–284.

[38] Z. Deng, J. Zhou, L. Miao, C. Liu, Y. Peng, L. Sun, S. Tanemura, J. Mater. Chem. A 5 (2017) 7691–7709.

[39] J.A. Barker, J. Biol. Educ. 30 (1996) 97–99.

[40] W. Jiang, H. Li, Z. Liu, Z. Li, J. Tian, B. Shi, Y. Zou, H. Ouyang, C. Zhao, L. Zhao, R. Sun, H. Zheng, Y. Fan, Z.L. Wang, Z. Li, Adv. Mater. 30 (2018) 1801895.

[41] Z. Liu, Y. Ma, H. Ouyang, B. Shi, N. Li, D. Jiang, F. Xie, D. Qu, Y. Zou, Y. Huang, H. Li, C. Zhao, P. Tan, M. Yu, Y. Fan, H. Zhang, Z.L. Wang, Z. Li, Adv. Funct. Mater. 29 (2019) 1807560.

[42] H.Y. Geng, Q. Xu, M.M. Wu, H.Y. Ma, P.P. Zhang, T.T. Gao, L.T. Qu, T.B. Ma, C. Li, Nat. Commun. 10 (2019) 1512.

[43] P. Zhang, F. Liu, Q. Liao, H. Yao, H. Geng, H. Cheng, C. Li, L. Qu, Angew. Chem. Int. Ed. 57 (2018) 16343–16347.

[44] P. Zhang, Q. Liao, H. Yao, Y. Huang, H. Cheng, L. Qu, Energy Storage Mater. 18 (2019) 429–446.

[45] H.D. Liu, X.T. Zhang, Z.X. Hong, Z.G. Pu, Q.Y. Yao, J.C. Shi, G.B. Yang, B.W. Mi, B. Yang, X. Liu, H.F. Jiang, X.J. Hu, Nano Energy 42 (2017) 115–121.

[46] S. Zhuang, L. Zhou, W. Xu, N. Xu, X. Hu, X. Li, G. Lv, Q. Zheng, S. Zhu, Z. Wang, J. Zhu, Adv. Sci. 5 (2018) 1700497.

[47] N. Xu, X. Hu, W. Xu, X. Li, L. Zhou, S. Zhu, J. Zhu, Adv. Mater. 29 (2017) 1606762.

[48] P. Tao, G. Ni, C. Song, W. Shang, J. Wu, J. Zhu, G. Chen, T. Deng, Nat. Energy 3 (2018) 1031–1041.

[49] H.Y. Jia, J. Wang, X.Y. Zhang, Y.P. Wang, ACS Macro Lett. 3 (2014) 86–90.

[50] Y. Jin, J. Chang, Y. Shi, L. Shi, S. Hong, P. Wang, J. Mater. Chem. A 6 (2018) 7942–7949.

[51] G. Ni, S.H. Zandavi, S.M. Javid, S.V. Boriskina, T.A. Cooper, G. Chen, Energy Environ. Sci. 11 (2018) 1510–1519.
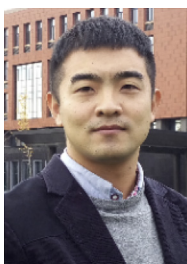
Dr. Peng Xiao received his Ph.D. in polymer chemistry and physics from Ningbo Institute of Materials Technology and Engineering, Chinese Academy of Sciences in 2017, under the supervision of Prof. Tao Chen. After that he joint Tao Chen's group as a postdoctoral research fellow. His current research interest focuses on the macroscopic self-assembly of 1D and 2D of carbon-based nanomaterials into 2D ultrathin films at air/water interface and further interfacial asymmetric modification to explore their potential applications in actuators, sensors and solar-to-thermal conversion.
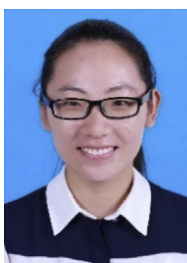
Jincui Gu received her MS degree in material science from Hainan University. In 2012, she joint Tao Chen's group as an assistant researcher. Her current research focuses on construction of the polymer functionalized carbon-based membranes for water purification.
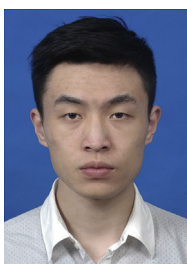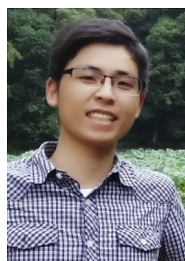

Chang Zhang received his B.S. degree from Ningbo Institute of Technology, Zhejiang University, China in 2016. Currently, he is a master candidate in the Ningbo University and the Ningbo Institute of Materials Technology and Engineering, Chinese Academy of Sciences, under the supervision of Prof. Wenqin Wang and Prof. Tao Chen. His research interests focus on the carbon-based hybrid materials toward application of photo-thermal conversion.

Feng Ni received his B.S. degree from Tianjin Polytechnic University in 2017. Currently, he is a PhD student in the Ningbo Institute of Materials Technology and Engineering, Chinese Academy of Sciences, under the supervision Professor Tao Chen. His current research interests focus on polymer/carbon-based 2D hybrid materials and photothermal conversion.

Yun Liang received his B.S. degree from Southwest University of Science and Technology. Currently, He is a PhD student in the Ningbo Institute of Materials Technology and Engineering, Chinese Academy of Sciences, under the supervision Professor Tao Chen and Youju Huang. His current research interests focus on polymer/Carbon-based 2D hybrid materials and their applications as sensors and actuators.

Jiang He received his M.S. degree from Ningbo University, China in 2016 under the supervision of Prof. Wenqin Wang from Ningbo University and Prof. Yousi Chen from Ningbo Institute of Materials Technology and Engineering, Chinese Academy of Sciences. Currently, he is a PhD student in the Ningbo Institute of Materials Technology and Engineering, Chinese Academy of Sciences, under the supervision of Prof. Tao Chen. His research interests focus on the smart polymers and carbon nano materials hybrid with applications as actuators and sensors.

Dr. Lei Zhang received his Ph.D. in chemical engineering from Zhejiang University in Nov. 2013. Then he joins the Prof. Tao Chen's group as a postdoctoral fellow in Ningbo Institute of Materials Technology and Engineering, Chinese Academy of Sciences. Afterwards he was promoted to associate professor in Dec. 2016. His current research is focused on the fabrication of functional polymer and their hybrids for the applications of stretchable electronics and smart actuators.

Prof. Jianyong Ouyang received his PhD, master and bachelor degrees from the Institute for Molecular Science in Japan, the Institute of Chemistry of the Chinese Academy of Science, and the Tsinghua university in Beijing, respectively. He worked as an assistant professor at the Japanese Advanced Institute of Science and Technology and a postdoctoral researcher at the University of California, Los Angeles (UCLA) before joining the National University of Singapore as an assistant professor in 2006. He was promoted to associate professor in 2012. His research interests include flexible electronics and energy materials and devices.

Prof. Shiao-Wei Kuo received his B.Sc. in chemical engineering from the National Chung Hsing University (1998) and Ph.D. in applied chemistry from the National Chiao Tung University in Taiwan (2002). He continued his research work at Chiao Tung University as a postdoctoral researcher during 2002–2007. Now, he is the professor in the Department of Materials and Optoelectronic Science, National Sun Yat-Sen University, Taiwan. His research interests include polymer interactions, self-assembly nanostructures, covalent organic frameworks, porous materials, POSS nanocomposites, polybenzoxazine, and polypeptides.

Prof. Tao Chen received his Ph.D. in polymer chemistry and physics from Zhejiang University in 2006. After his postdoctoral training at the University of Warwick (UK), he joined Duke University (USA) as a research scientist. He then moved back to Europe as an Alexander von Humboldt Research Fellow at Technische Universität Dresden, Germany. Since 2012, he is a full-time professor at Ningbo Institute of Materials Technology and Engineering, Chinese Academy of Sciences. His research interests include smart polymers and their hybrid systems with applications as actuators, shape memory polymers, and chemical sensing.